Materials Characterization 145 (2018) 347–352

Contents lists available at ScienceDirect

Materials Characterization

journal homepage: www.elsevier.com/locate/matchar

Nanoscale analysis of dispersive ferroelectric domains in bulk of hexagonal multiferroic ceramics

Ali Baghizadeh[a,*], Joaquim M. Vieira[a], Daniel G. Stroppa[b,1], Marc-Georg Willinger[c,2], Vitor S. Amaral[d]

[a] Department of Materials & Ceramic Engineering & CICECO Institute of Materials, Aveiro University, 3810-193 Aveiro, Portugal
[b] Quantitative Electron Microscopy Group, International Iberian Nanotechnology Laboratory, 4715-330 Braga, Portugal
[c] Department of Inorganic Chemistry, Fritz Haber Institute of the Max Planck Society, Faradayweg 4-6, Berlin, Germany
[d] Department of Physics & CICECO Institute of Materials, Aveiro University, 3810-193 Aveiro, Portugal

ARTICLE INFO

Keywords:
Ferroelectric domains
Aberration corrected STEM
Defective lattices
Multiferroic oxides

ABSTRACT

The atomic nature of topologically protected ferroelectric (FE) walls in hexagonal $ReMnO_3$ oxides (R: Sc, Y, Er, Ho, Yb, Lu) creates an interesting playground to study effects of defects on domain walls. The 6-fold FE vortices in this multiferroic family lose the ordering by the rule of 6 in the presence of partial edge dislocations (PED) besides it can be modified by chemical doping. Therefore, it is essential to comprehend the cross coupling of FE walls and defects or vacancies in the lattice of multiferroics. Atomic resolution STEM is used to explore the correlative response of electrical polarization of FE domains in the presence of defects in multiferroic ceramics. Such level of resolution also allows the study of switching of FE domains on encounter of lattice defects. The driving force behind appearance of dispersed, small FE domains in images of piezo force microscopy is revealed by observation of lattice defects and FE boundaries simultaneously at the nano-scale. Planar defects and FE domain walls play their role of internal interfaces consequently such interplaying duly modifies the magnetic and FE properties of multiferroic oxides.

1. Introduction

Recent appearance of interlocking of ferroelectric domain walls and structural anti-phase boundaries in hexagonal lattices of $RMnO_3$ oxides pushed researchers to investigate properties of FE domains and rules governing their emergence [1–4]. It was shown that 6-fold vortices, also called cloverleaf patterns, consist of 6 FE domains of which the polarization direction (displacement of R ions with 4b Wyckoff sites) is reversed upon crossing the domain wall. Lattice energy at structural antiphase domain boundaries created at trimerization stage is decreased by switching the direction 4b R^{3+} ion displacements in coincidence with the phase shift by in-plane displacement of apical oxygen ions [2].

Vacancy doping of Mn or Lu cation sites duly modifies multiferroic properties of self-doped h-$LuMn_xO_{3\pm\delta}$ ceramics, as previously shown by one of us, where it was also found that self-poling introduces point defects in the lattice which interact with FE domain walls [5]. Manipulation of 6-fold FE vortices in h-$RMnO_3$ oxides has been achieved via controlled cooling rate [1], doping the lattice [6–8], oxygen vacancies [9,10] and mechanical strain [11]. The atomically sharp nature of FE domain walls makes their study feasible only with nano-analytic tools like TEM/STEM of sub-angstrom resolution to display R ion displacements and right identification of grains with adequate crystal orientation if one works with bulk ceramics [12,13]. These issues became the object of current research employing probe-corrected STEM to get distinct representations of FE domain switching upon meeting extended lattice defects in vacancy disordered lattices. Rare studies on polarization switching, or phase shifting of FE domains in the presence of lattice defects demand further investigation. To gain additional insight into interactions of defects and FE domain walls, self-doped ceramics with off-stoichiometric composition of either Lu, or Mn excess were selected for this study.

* Corresponding author.
E-mail addresses: ali.baghizhadeh@ua.pt (A. Baghizadeh), jvieira@ua.pt (J.M. Vieira), Daniel.Stroppa@fei.com (D.G. Stroppa), marc.willinger@scopem.ethz.ch (M.-G. Willinger).
[1] Current address: Materials & Structural Analysis, Thermo Fisher Scientific, Achtseweg Noord 5, Bldg. III 1-155 5651 GG Eindhoven, The Netherlands.
[2] Current address: Scientific Center for Optical and Electron Microscopy-ScopeM, ETH Zürich, 8093 Zürich, Switzerland.

https://doi.org/10.1016/j.matchar.2018.08.042
Received 23 May 2018; Received in revised form 17 July 2018; Accepted 23 August 2018
Available online 26 August 2018

2. Experimental Section

2.1. Sintering of Ceramics

The solid state reaction method with suitable mixing of the Lu_2O_3 (99.999%) and MnO_2 (99.999%) oxides was used to produce ceramic pellets. Firing of samples was done in three steps with intermediate grinding, ended at 1300 °C after 5 days annealing in air to obtain properly reacted ceramics [14]. All sintered ceramics present the $P6_3cm$ space group as main phase within the detection limit of XRD analysis (supplementary materials, Fig. S1).

2.2. Microscopy Analysis

TEM/STEM sample preparation was done by mechanical polishing down to 10 μm controlled by silicon transparency followed by gentle Ar^+ ion milling. Preliminary TEM analysis was done with the JEOL JEM2200FS FEG 200 kV electron microscope. HAADF-STEM images of sub-Angstrom resolution were taken using the C_s/probe-corrected Titan Themis TEM/STEM microscope operated at either 200 kV or 300 kV, 30 mrad convergence angle and over 80 mrad collection angle for HAADF detector.

3. Results and Discussion

Displacement of Lu ions in the HAADF-STEM image along [110] zone axis of sample $LuMn_{0.96}O_{3\pm\delta}$ in Fig. 1a is well resolved and shows upward FE polarization by Lu displacement [12]. Mn ions fill rows of weaker contrast between the rows of Lu ions in agreement to the $P6_3cm$ crystalline structure of $LuMnO_3$ phase. Close observation of the image revealed a boundary separating the regular hexagonal lattice of $P6_3cm$ symmetry (above) from a monoclinic-like distortion of the lattice (bellow) with c-axis tilted by approximate 2° in relation to the orthogonal direction with a-b plane, the orthogonal being given by the yellow line in Fig. 1a. In the upper half of the image the yellow line overlaps with the origin of FE periods. The white line on low-right gives the change in position of origin of corresponding FE periods in c-axis-tilted area. Border between the two areas coincides with anomalous

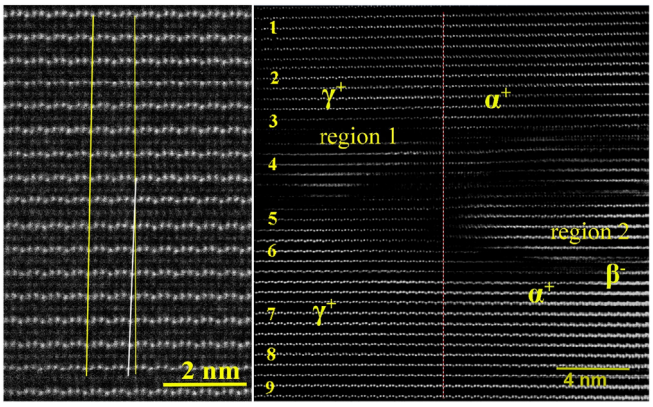

Fig. 1. HAADF-STEM images along [110] zone axis of two regions of a grain h-$LuMn_xO_{3\pm\delta}$ ceramics with x = 0.96 composition. a) One (001) boundary plane separates the regular hexagonal $LuMn_{0.96}O_{3\pm\delta}$ lattice (above) from distortion of hexagonal lattice with monoclinic axis (white line on right) with α = 90°, β ≅ 87.7° and γ = 120° showing a partial dislocation ribbon. b) HAADF-STEM image of the defective region of the same crystalline grain of (a). FE domains of same polarization direction, but of different phase are observed (indicated as α^+ and β^+). From left to right of the image, a low angle boundary of 1.12° rotates the planes of Lu ions under the effect underlying stacking faults. Areas marked 1 and 2 will be object for further analysis in Fig. 2. Numbers on the left of image give the atomic planes selected for calculation of ionic polarization along the vertical dash line in the middle of the figure.

interspacing of Lu-planes 20% wider than the regular spacing of the Lu planes. White line meets the reference yellow line at this boundary plane. The end of the lines on the low-right marks the position where the crystalline lattice returned to regular hexagonal alignment, the width of tilted band being approximately $4c_0$ (c_0, the c-constant of the unit cell). Development of this slightly tilted band of narrow width in the lattice of $LuMn_{0.96}O_{3\pm\delta}$ bears remarkable similarity with dislocation structures of another hexagonal lattice of ionic species, the crystalline lattice of corundum, the α-Al_2O_3, where gradual displacement of O^{2-} ions in the $[1\bar{2}10]$ direction of the quarter partial dislocation gliding in the basal plane is linked to simultaneous shift of Al^{3+} interstitials in octahedral sites, the gradual displacement of ions being distributed by fractional displacements over a dozen consecutive planes of the dislocation ribbon [15]. The Burger vector of displacement of the regular lattice of $LuMn_{0.96}O_{3\pm\delta}$ on upper half of Fig. 1a slipped by $\overrightarrow{b_p}$ in relation to the unslipped lattice bellow the tilted band is approximately $\overrightarrow{b_p} \cong 1/6[1\bar{1}0]$. The width $4c_0$ of the partial dislocation ribbon yields the shear strain $|\overrightarrow{b_p}|/c_0$ of 3.8% and shear angle 2.2°.

Examination of other areas of same particle showed defective areas with stacking faults and revealed switching FE polarization direction from upward to downward at several places. Also, analysis of Lu ion displacements shows phase shift along atomic planes of Lu ions with the constant FE polarization direction which breaks the ground rule of 6-fold vortices but is permitted by the presence of partial dislocations and correlated planar defects of crystalline lattices [8,16].

The strain field of a probable stacking fault in the center of Fig. 1b caused the phase shift of FE domains above and below the defect. Considering α^+ the phase of FE domains on the right side there is gradual change in the azimuthal angle which determines the phase of FE domains, ending in the γ^+ phase on the left [12] (Fig. S2 shows the phase shift from one domain to another one using a scale to determine the phase shift). Since this angle is defined by the shifting of the direction of apical oxygen from α^+ [2], appearance of a second phase with the same polarization of FE domains uncovers the effect of stacking fault on the tilting of MnO_5 bipyramids which resulted in breaking the rule of 6-fold vortices. FE vortices of different phase but one same polarization would not be energetically favorable in a regular h-$RMnO_3$ lattice [2]. But, the appearance of a phase shift in FE domains of fixed polarization direction in the lattice of $YMnO_3$ and $Y_{0.67}Lu_{0.33}MnO_3$ single crystals was explained by the concomitant presence of a partial edge dislocations (PED) coupled to vortex lines [8,16]. In aforementioned studies, on the boundary of the FE domains with same polarization, extra (030) atomic planes of the PEDs were detected thus creating phase shifts in the lattice. The PED's appeared linked to vortex cores whenever the lattice lost the ground symmetry of regular trimerization.

Although no evidence of extra atomic planes is found by moving from below to top of the image in Fig. 1b, twisting of Lu planes by 1.12° is detectable. On the right side of the defect polarization switching is not seen except at the low right corner, continued as Fig. 2a, where β^- phase appears, the domain wall (marked by the dashed line in this figure) is of type I (1/3 of unit cell) [13]. This domain wall displays combination of DW perpendicular to the polarization direction (transversal domain wall, TDW) and DW parallel to the polarization direction (longitudinal domain wall, LDW), a domain wall of type C [17]. This region of reverse polarization is small. It can be considered a nano-FE domain of negative polarization immerging in a composite area of positive polarization.

Split planes of Lu ions with positive and negative polarization facing each other were found at the border in region of Fig. 1b, propagated to the left and enlarged in Fig. 2b. The distance between two Lu planes of opposite polarization in the split pairs of the disordered region ranges from 0.15 nm to 0.23 nm in average and looks insufficient to interleave any Mn plane between them. The specific contrast of Mn planes in non-defective regions is missing in the image of Fig. 2b. In the regular lattice

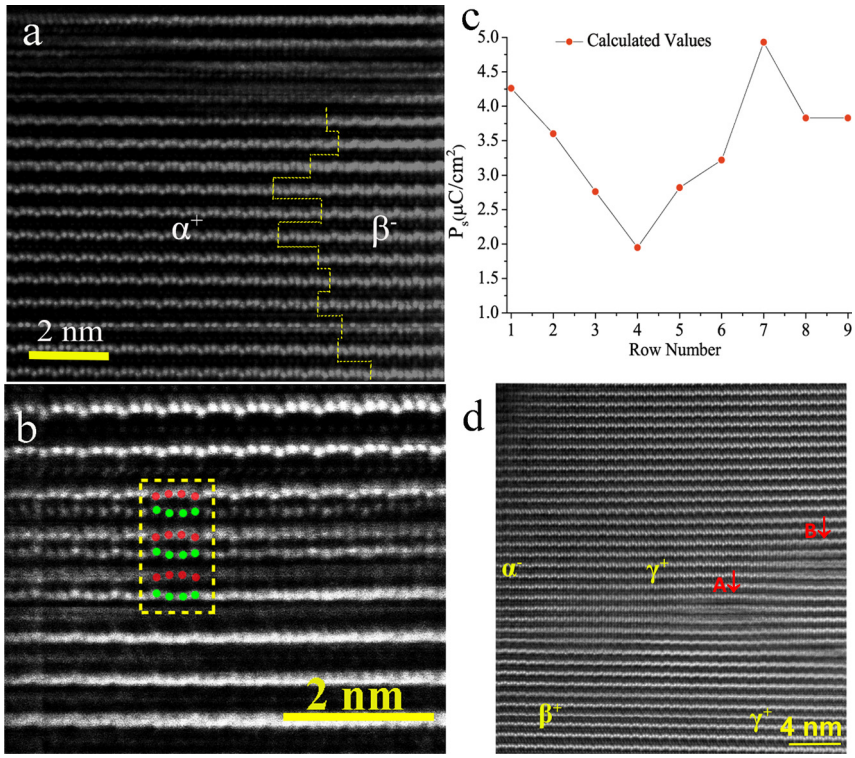

Fig. 2. a) FE polarization switching in the vicinity of the stacking fault in Fig. 1b, region 2, the dash, lines in yellow indicate the position of APB-FE domain walls between two FE domains. b) Enlarged view of the defect in region 1 of Fig. 1b with stacking fault formed by assemblage in a triple-layered structure of split pairs of Lu planes with mutual cancelation of FE polarization and of total stacking fault displacement, $\overrightarrow{b_P} = {}^1/_6[001]$. Inside the dash box in yellow color in the image, red dots and green dots show the positive negative polarization of Lu ions, respectively. c) Calculated values of ionic polarization P_s (Eq. (1)) along the vertical dash line in Fig. 1b revealing changes in FE polarization from high values in regular lattice sites to lower values in defective regions. Additional information can be found in supplementary materials, Fig. S2. d). Image from the left side of stacking fault in Fig. 1b in the edge of TEM thin section showing presence of antiphase FE domains, switching of polarization in a narrow region and nuclei of split pairs of Lu planes (A, B). (For interpretation of the references to color in this figure legend, the reader is referred to the web version of this article.)

of h-$LuMn_{0.96}O_{3\pm\delta}$, Fig. 1a, distance along c-axis of two successive Lu planes is 0.55 nm, the distance between Lu and Mn planes being half of this value. This is a Mn deficient composition of $LuMn_xO_{3\pm\delta}$ ($x < 1$) where Mn^{3+} vacancies ($V_{Mn}^{'''}$) may form to assure point defect balance with electrical neutrality in the crystalline lattice. Condensation of $V_{Mn}^{'''}$ vacancies can create a stacking fault limited by two partial dislocations which roughly removes one Mn-O layer in the extension of the stacking fault. Loss of the Mn-O plane with connected planar oxygen ions may constitute the chemical driving force for appearance a new atomic structure which is tentatively explained as follows.

Point defect interaction in the lattice of $LuMn_xO_{3\pm\delta}$ samples with $x < 1$ favors clustering of excess, namely of $V_{Mn}^{'''}$, in very localized regions expected from decreasing point defect solubility in the lattice during cooling. Loosing of Mn ions in the center of some MnO_5 bipyramids breaks charge neutrality in the unit cell. Polarization switching in the pair of Lu split planes would be energetically favored because besides decreasing net electric polarization energy density it also keeps Lu^{3+} (4b) ions far apart in the two Lu planes. The alternative with the same Lu displacement in the unit cells of successive atomic planes brings both Lu ions of (4b) and (2a) Wyckoff positions to close distances. Repulsive columbic interactions between Lu^{3+} ions in short spaced Lu planes certainly makes the alternative arrangement less probable to occur. Some similarity and analogy must be point out between the switching of polarization of Lu ions in the atomic structure found in h-$LuMn_{0.96}O_{3\pm\delta}$ ceramics, shown in Fig. 2b, and the one reported for $(LuFeO_3)_m/(LuFe_2O_4)_1$ ($1 \le m \le 10$) supperlattices deposited by reactive-oxide molecular beam epitaxy [18]. As in the h-$LuMnO_3$ structure showed in Fig. 2b, h-$LuFeO_3$ planes of $(LuFeO_3)/(LuFe_2O_4)$ interfaces on both sides of the $(LuFe_2O_4)_1$ layer of superlattices with $m \ge 2$ display trimerization with symmetrical directions of polarization in tail-to-tail configuration while one APB-FE domain wall closely parallel to the interface always forms inside the $(LuFeO_3)_m$ layers splitting them into two FE stripes in head-to-head configuration of polarization, as seen in (Fig. 1b, ref. [18]). Electronic charge movement from $(LuFe_2O_4)_1$ layer to the $LuFeO_3$ phase increases the stability of charged APB-FE domain walls in doped-type structures of the superlattice. $LuFe_2O_4$ in the ferroelectric charged order state, Cm space group, is a charge ordered weak ferroelectric driven by co-existence of Fe^{2+} and Fe^{3+} in two Fe-O planes between single Lu-O planes of the unit cell [18]. Arrangement of Lu ions in Lu-O planes of ferroelectric charge ordered state of $LuFe_2O_4$ matches the one of Lu-O planes in trimerized h-$LuFeO_3$ of $P6_3cm$ crystalline structure and makes the $(LuFeO_3)/(LuFe_2O_4)$ interface coherent. For $m = 6$ and $m = 7$ superlattices (Fig. 1b, ref. [18]), displacements of Lu ions in the Lu-O layer of one interface of $(LuFe_2O_4)_1$ mirrors the positions of ions in the opposite interface while in remaining superlattices of $(LuFeO_3)_m/(LuFe_2O_4)_1$ ($2 \le m \le 10$) a shift of phase of the trimerized h-$LuFeO_3$ structure is observed on each side the $(LuFe_2O_4)_1$ layers. Along one $(LuFe_2O_4)_1$ layer mirroring of Lu positions commutates to phase stepped configuration of polarization of the Lu-O planes of the interfaces when the APB-FE domain wall moves from inside the $(LuFeO_3)_m$ layer towards the interface with $(LuFe_2O_4)_1$ where it terminates (extended data Fig. 5, ref. [18]). Reversal of FE polarization direction across the $(LuFe_2O_4)_1$ layers and concurrent splitting of each $(LuFeO_3)_m$ layer in two FE stripes decrease the electric polarization energy density of the superlattice.

The role of the oxygen vacancy in topology breaking by introducing new patterns of APB/FE domains besides of 6-fold vortices was recently demonstrated in h-$RMnO_3$ single crystals and resulted in 4-fold vortices, vortex core fragmentation and stripe patterns [3,9,10,19]. Results of density functional calculations demonstrated that introducing apical oxygen vacancies in the structure of $InMnO_3$ converts the $P6_3cm$ crystal structure to P_3c1 type structure [20,21]. Yet, displacements of Lu ions in Fig. 2b still follow the $P6_3cm$ crystalline structure of undistorted regions. Oxygen vacancy concentration must increase in proportion to $V_{Mn}^{'''}$ concentration in Mn deficient $LuMn_xO_{3\pm\delta}$ samples ($x < 1$), when these point defects dominate the electrical neutrality condition $2[V_O^{\cdot\cdot}] \approx 3[V_{Mn}^{'''}]$. Arrangement of Lu displacements in the three pairs of Lu-O split planes in Fig. 2b exhibits a tail-to-tail FE boundary (where the displacement of the Lu ions on both sides of the domain wall is in opposite directions) in a width of just two atomic planes along c-axis with parallel head-to-head FE polarization in the spaces left between pairs of Lu-O split planes. The analogy with the tail-to-tail FE boundary played by the $(LuFe_2O_4)_1$ layers interleaved in $(LuFeO_3)_m$ layers of the

superlattice ceases here, the atomic distance between Lu-O planes in split pairs being too narrow to hold a single plane of a different phase.

Ionic polarization (P_s) is calculated by quantification of variations in displacement of Lu ion along atomic rows labelled with numbers in Fig. 1b [22]. Displacements of Lu (4b) and Lu (2a) ions of 4 unit cells in each atomic row around the vertical dashed line are measured. Ionic polarization of a unit cell is calculated as [22]:

$$P_s\left(\frac{\mu C}{cm^2}\right) = \left(\sum Z_i^* \Delta c_i\right)\Big/_V \quad (1)$$

where Δc_i is the displacement of Lu ions along c-axis from the centrosymmetric position, Z_i^* are the Born effective charge of Lu ions (3.6 e for Lu sites) and V, volume of the unit cell [22,23]. Values of P_s are plotted in Fig. 2c. The average of P_s along atomic rows in non-distorted unit cells (points 1, 2, 8 and 9 in Fig. 1b and S3) gives 3.8 μC/cm^2, close to 3.72 μC/cm^2 determined from the unit cell (supplementary materials, Table S1). A net drop in local polarization P_s to an average 2.7 μC/cm^2 clearly appears in Lu planes located in, or very close to stacking faults. Such a local degradation in ionic polarization was observed in $YMnO_3$ single crystals because of oxygen vacancies [22]. Atomistic simulation of oxygen deficient domain walls in the $YMnO_3$ lattice revealed unit cell distortion at domain walls accompanied by drop in local ferroelectric polarization [24]. Titling of MnO_5 bipyramids and buckling of Lu planes induced by the point defects, which in turn modify ferroelectric polarization, has also support of theoretical calculations [25,26]. Analysis of local ionic polarization on the ribbon dislocation in Fig. 1a did not result in measurable variation in P_s in comparison to values of P_s of the regular lattice. The ribbon dislocation changed atomic arrangements of the Lu ions along Lu rows (parallel to a-b plane) but, the stacking fault disturbs assembling of Lu planes along polarization direction itself. Switching of Lu displacement with emerging paired-spit of Lu-planes is also observed in the isolated volume of lens-shape (A) and the edge (B) of the TEM thin section (Fig. 2d). Left to the stacking fault in Fig. 1b, Lu-O planes regain the regular lattice structure in approaching the TEM thin section edge where the polarization changes from up in the right to down in the left, accompanied with phase shift from γ^+ to α^-, Fig. 2d. The γ^+ phase changes to β^+ phase in Fig. 2d as in vicinity of stacking fault the lattice spacing is modified by the strain field of the planar defect. Adding images in Figs. 1b and 2d, both from the lower part of the same stacking faulted area, one counts three phase shifts inside a multipart area with fixed (+) polarization, from α^+ to γ^+ and then to β^+ (from right of the defect to the left, and edge of the particle thin section). The analogous feature described in h-$RMnO_3$ oxides is the direct result of the complex energy scheme of topological defects in defective lattices [16]. Change in lattice energy of hexagonal topological defects by creating local poling of applied electric fields [27] or by self-poling of oxygen [9] disturbs the topological features of 6-fold vortices with cloverleaf patterns of FE domains and yields core fragmentation, appearance of very thin FE domains, or head-to-head domain walls inside the same trimerization antiphase. Partial edge dislocations in the h-$RMnO_3$ oxides also resulted in the presence of same polarization of different antiphase domains without the corresponding domain walls [8].

Further insight into the nature of defects presented in disordered lattices of h-$RMnO_3$ materials and their interaction with FE topological defects is gained from the analysis of the sample with Mn excess. Fig. 3a shows an anti-phase boundary in a crystalline grain of $LuMn_{1.04}O_{3\pm\delta}$ aligned to [110] zone axis. The structural APB propagated from the free edge of grain to well inside the particle ending in a stacking fault causing the strain of lattice planes seen in Fig. 3b. The same direction of downward FE polarization is retained along the trace of the APB and on both sides. Phase analysis of FE domains in both sides at the termination of APB in Fig. 3b shows phase shifting from α^- in left to γ^- in right. Crystalline planes on both sides of the APB are slightly tilted by 0.3°–1°. Fig. 3a and b give atomic resolution HAADF-STEM images of the APB equivalent to APB structure observed in TEM images of lattice

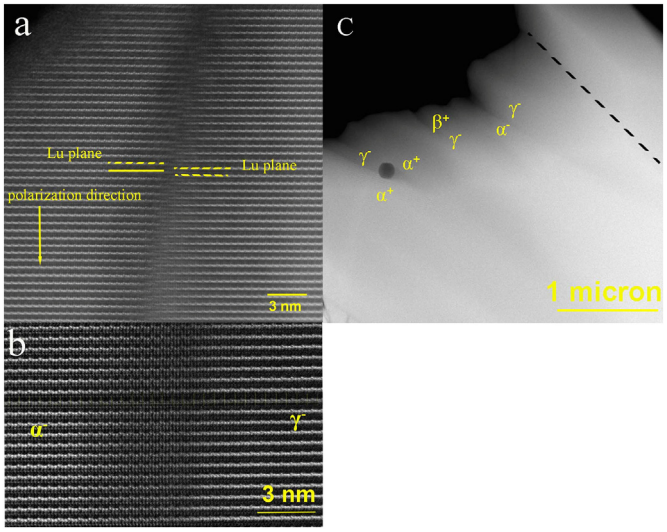

Fig. 3. HAADF-STEM image of the lattice of $LuMn_{1.04}O_{3\pm\delta}$ ceramic with Mn excess. a) Structural anti-phase boundary which begins at the surface of the particle and ends down inside the crystalline grain. b) Lattice strain at the APB ends, the strain field leading to phase shift of the FE domain while (downward) polarization direction is maintained. c) Low magnification STEM image of crystalline grain with size below 3 μm revealing the mapping of FE polarization direction and phases (dash line in black indicates the position of the high angle grain boundary with the neighboring grain particle).

resolution of epitaxial thin films of h-$DyMnO_3$ on $ZrO_2(Y_2O_3)$ (111) substrates [28]. The APB surface in Fig. 3a is vicinal to the plane parallel to [110] zone axis and slanted by approximately 11° to the c-axis direction. The component of the displacement vector of SF parallel to c-axis is 1/4[001]. Such rearrangement of the Mn planes disturbs spin ordering in antiferromagnetic state, requiring further theoretical support to be modelled as supercell of broken symmetry lattices.

Generated by substrate monolayer steps the APBs of h-$DyMnO_3$ thin film observed were vertical or inclined by 15° and 25° to c-axis direction [28]. Pyramidal planes in the hexagonal lattice of $RMnO_3$ which are parallel to the [110] zone axis and tilted by 15° and 25° to c-axis display large densities of Mn and Lu sites. Subdomains observed in h-$DyMnO_3$ thin film were considered as result from π/3 rotations in basal plane coupled to shifts of c/6 or even of c/3 in c-axis direction. An idealized model for APBs of h-$DyMnO_3$ thin film with displacement of c/6 in the c-axis direction had been proposed [28]. Intensity of *Z*-contrast of HAADF-STEM images is a parabolic function of the atomic number of the atoms. The hexagonal lattice provides equivalent orientations for each type of pyramidal planes around c-axis of 6-fold symmetry. One recognizes that in STEM images in Fig. 3, overlapping of two wedged parts of opposite polarization in tail-to-tail FE walls may also create images with paied Lu-O split planes. The two wedged parts are separated by a pyramidal APB, where the APB is inclined in relation to the [110] zone axis and is tilted to the c-axis, the two wedged parts are shifted by $^1/_6$[001]. The structures of small domains (or clusters) as in Fig. 1b would demand a more elaborated explanation and may come from APBs encircled by the PED loops. Point defect condensation or shift of lattice blocks along APBs were presented as probable origin of paired Lu-O split planes in the lattice of h-$LuMnO_3$ described in this study but, one cannot securely separate them with the limited data so far available.

Phase shift in the immediate vicinity of a linear defect (the PED) as it was observed in the lattice of $Y_{0.67}Lu_{0.33}MnO_3$ single crystals replicates the observation in Fig. 1b [8]. The phase and polarization direction of FE domains in different places of the particle being investigated are shown in Fig. 3c (the low magnification image of the crystalline grain in Fig. 3a and b). The particle of approximately 2 μm

wide contains two main FE antiphase domains, α^+ and γ^-, with a narrow region of β^+ phase at the free edge of the particle, and α^- phase generated by the APB in Fig. 3a and b. Investigating the FE domains by PFM technique in the same vacancy doped ceramics ($x > 1$) of this study revealed large FE domains wider than 1 μm (supplementary materials, Fig. S4). However, in the same PFM images much smaller FE domains of sizes below 1 μm were found dispersed inside large FE domains of opposite polarization direction [29]. Within the detection limits of the technique of the EDS analysis, this particle showed no evidence of variation in chemical composition [29]. The PFM observations are corroborated by the dimensional scale of FE domain map in Fig. 3c, where quite small FE domains appeared in just the same grain. The distributed slip of a ribbon PED, the lattice strain of planar defects namely of stacking faults and structural anti-phase boundaries are extrinsic features, extended defects found in the crystalline lattice h-$LuMn_xO_{3\pm\delta}$ ceramics that modify the phase of trimerization and FE polarization direction and substitute topological APB-FE domains. Large densities of such extended defects in the strain lattices of bulk h-$RMnO_{3\pm\delta}$ multiferroics will impress the corresponding dimensional scale to the spatial distribution of FE domains and easily preclude the observation of topological vortices with density regulated by intrinsic mechanisms of topological phase transitions [30].

4. Conclusion

In summary, intentionally introduced vacancies of the lattice of h-$LuMn_xO_{3\pm\delta}$ ceramics were used to expand current understanding on the effect of lattice defects on FE domains/walls. It was shown that stacking faults may effectively suppress local electrical polarization of the unit cell. This can be generalized to any extended defect which disturbs stacking sequences of Lu planes along c-axis. The presence of FE domains of same polarization but different phases was observed in defective lattices which gave rise to new evidence on violating the ground rule of 6 in topological vortices driven by the lattice defects. Vacancy condensation in small regions was shown to induce FE switching in few atomic planes. It results in new insight into the effect of point defects on ferroelectricity in FE materials. Besides of partial edge dislocations which reduce topology from 6-fold to 4-fold truncated vortices, the set of extended defects with topology breaking impact in polycrystalline h-$RMnO_3$ materials is widening: grain boundaries as based on PFM analysis, ribbon dislocations, stacking faults with associated structural antiphase boundaries and atom clusters created by segregation due to fluctuation of chemical composition. Exploring main interactions between defects and FE domains in h-$RMnO_3$ oxides and the envisaged expansion to h-$RFeO_3$ oxides become of great importance in film technology where lattice defects modify ferroelectric domains and domain walls accordingly. Consequently, pinning of antiferromagnetic and FE walls and magnetoelectric coupling are expected to sense the interaction of ferroelectricity and defects.

Data Availability Statement

The raw/processed data required to reproduce these findings cannot be shared at this time as the data also forms part of an ongoing study. They can be shared upon request.

Declarations of Interest

None. There is nothing to be declared regarding the submitted manuscript.

Acknowledgements

A. B. acknowledges the FCT fellowship SFRH/BDP/115625/2016. This work was developed within the scope of the project CICECO-Aveiro Institute of Materials, POCI-01-0145-FEDER-007679 (FCT Ref. UID/CTM/50011/2013), financed by national funds through the FCT/MEC and when appropriate co-financed by FEDER under the PT2020 Partnership Agreement.

Appendix A. Supplementary data

Supplementary data to this article can be found online at https://doi.org/10.1016/j.matchar.2018.08.042.

References

[1] M. Lilienblum, T. Lottermoser, S. Manz, S.M. Selbach, A. Cano, M. Fiebig, Ferroelectricity in the multiferroic hexagonal manganites, Nat. Phys. 11 (2015) 1070–1073, https://doi.org/10.1038/nphys3468.
[2] Y. Kumagai, N.A. Spaldin, Structural domain walls in polar hexagonal manganites, Nat. Commun. 4 (1) (2013), https://doi.org/10.1038/ncomms2545.
[3] S.C. Chae, Y. Horibe, D.Y. Jeong, S. Rodan, N. Lee, S.-W. Cheong, Self-organization, condensation, and annihilation of topological vortices and antivortices in a multiferroic, Proc. Natl. Acad. Sci. U. S. A. 107 (2010) 21366–21370, https://doi.org/10.1073/pnas.1011380107.
[4] H. Das, A.L. Wysocki, Y. Geng, W. Wu, C.J. Fennie, Bulk magnetoelectricity in the hexagonal manganites and ferrites, Nat. Commun. 5 (2014) 1–11, https://doi.org/10.1038/ncomms3998.
[5] A. Baghizadeh, J.M. Vieira, J.N. Gonçalves, M.G. Willinger, M.C. Ferro, V.S. Amaral, Nano-domains coupled to FE domains induced by lattice distortion in self-doped $LuMn_xO_{3\pm\delta}$ hexagonal ceramics, J. Phys. Chem. C 120 (2016) 21897–21904, https://doi.org/10.1021/acs.jpcc.6b04478.
[6] E. Hassanpour, V. Wegmayr, J. Schaab, Z. Yan, E. Bourret, T. Lottermoser, M. Fiebig, D. Meier, Robustness of magnetic and electric domains against charge carrier doping in multiferroic hexagonal $ErMnO_3$, New J. Phys. 18 (2016) 043015, https://doi.org/10.1088/1367-2630/18/4/043015.
[7] M.H. Harunsani, J.Q. Li, Y.B. Qin, H.T. Tian, J.Q. Li, H.X. Yang, R.I. Walton, Spontaneous formation of circular and vortex ferroelectric domain structure in hexagonal $YMnO_3$ and $YMn_{0.9}Fe_{0.1}O_3$ prepared by low temperature solution synthesis, Appl. Phys. Lett. 107 (2015) 062905, https://doi.org/10.1063/1.4928565.
[8] Q.-H. Zhang, G.-T. Tan, L. Gu, Y. Yao, C.-Q. Jin, Y.-G. Wang, X.-F. Duan, R.-C. Yu, Topology breaking of the vortex in multiferroic $Y_{0.67}Lu_{0.33}MnO_3$, Appl. Phys. Lett. 105 (2014) 012902, https://doi.org/10.1063/1.4887057.
[9] X. Wang, F.-T. Huang, R. Hu, F. Fan, S. Cheong, Self-poling with oxygen off-stoichiometry in ferroelectric hexagonal manganites, APL Mater. 3 (2015) 041505, https://doi.org/10.1063/1.4908159.
[10] Y. Du, X. Wang, D. Chen, Y. Yu, W. Hao, Z. Cheng, S.X. Dou, Manipulation of domain wall mobility by oxygen vacancy ordering in multiferroic $YMnO_3$, Phys. Chem. Chem. Phys. 15 (2013) 20010–20015, https://doi.org/10.1039/c3cp52892h.
[11] X. Wang, M. Mostovoy, M.G. Han, Y. Horibe, T. Aoki, Y. Zhu, S.-W. Cheong, Unfolding of vortices into topological stripes in a multiferroic material, Phys. Rev. Lett. 112 (2014) 1–5, https://doi.org/10.1103/PhysRevLett.112.247601.
[12] Q.H. Zhang, L.J. Wang, X.K. Wei, R.C. Yu, L. Gu, A. Hirata, M.W. Chen, C.Q. Jin, Y. Yao, Y.G. Wang, X.F. Duan, Direct observation of interlocked domain walls in hexagonal $RMnO_3$ (R = Tm, Lu), Phys. Rev. B 85 (2012), https://doi.org/10.1103/PhysRevB.85.020102 020102(R).
[13] M.-G.G. Han, Y. Zhu, L. Wu, T. Aoki, V. Volkov, X. Wang, S.C. Chae, Y.S. Oh, S.-W.W. Cheong, Ferroelectric switching dynamics of topological vortex domains in a hexagonal manganite, Adv. Mater. 25 (2013) 2415–2421, https://doi.org/10.1002/adma.201204766.
[14] A. Baghizadeh, J.M. Vieira, D.G. Stroppa, P.M. Vaghefi, M.P. Graça, J.S. Amaral, M.-G. Willinger, V.S. Amaral, Interaction of multiferroic properties and interfaces in hexagonal $LuMnO_3$ ceramics, J. Phys. D. Appl. Phys. 50 (2017) 055304, https://doi.org/10.1088/1361-6463/50/5/055304.
[15] S. Amelinckx, Structural aspects of stacking faults and fault propagation of the fine structure of dislocations, J. Phys. Colloq. 35 (1974), https://doi.org/10.1051/jphyscol:1974701 C7-1-C7-33.
[16] S. Cheng, J. Li, M.-G. Han, S. Deng, G. Tan, X. Zhang, J. Zhu, Y. Zhu, Topologically allowed nonsixfold vortices in a sixfold multiferroic material: observation and classification, Phys. Rev. Lett. 118 (2017) 145501, https://doi.org/10.1103/PhysRevLett.118.145501.
[17] L. Tian, Y. Wang, B. Ge, X. Zhang, Z. Zhang, Direct observation of interlocked domain walls and topological four-state vortex-like domain patterns in multiferroic $YMnO_3$ single crystal, Appl. Phys. Lett. 106 (2015) 112903, https://doi.org/10.1063/1.4915259.
[18] J.A. Mundy, C.M. Brooks, M.E. Holtz, J.A. Moyer, H. Das, A.F. Rébola, J.T. Heron, J.D. Clarkson, S.M. Disseler, Z. Liu, A. Farhan, R. Held, R. Hovden, E. Padgett, Q. Mao, H. Paik, R. Misra, L.F. Kourkoutis, E. Arenholz, A. Scholl, J.A. Borchers, W.D. Ratcliff, R. Ramesh, C.J. Fennie, P. Schiffer, D.A. Muller, D.G. Schlom, Atomically engineered ferroic layers yield a room-temperature magnetoelectric multiferroic, Nature 537 (2016) 523–527, https://doi.org/10.1038/nature19343.
[19] Y. Du, X.L. Wang, D.P. Chen, S.X. Dou, Z.X. Cheng, M. Higgins, G. Wallace, J.Y. Wang, Domain wall conductivity in oxygen deficient multiferroic $YMnO_3$ single crystals, Appl. Phys. Lett. 99 (2011) 252107, https://doi.org/10.1063/1.3671393.
[20] S.M. Griffin, M. Reidulff, S.M. Selbach, N.A. Spaldin, Defect chemistry as a crystal

structure design parameter: intrinsic point defects and Ga substitution in $InMnO_3$, Chem. Mater. 29 (2017) 2425–2434, https://doi.org/10.1021/acs.chemmater.6b04207.
[21] F.-T. Huang, X. Wang, S.M.M. Griffin, Y. Kumagai, O. Gindele, M.-W. Chu, Y. Horibe, N.A.A. Spaldin, S.-W. Cheong, Duality of topological defects in hexagonal manganites, Phys. Rev. Lett. 113 (2014) 267602, https://doi.org/10.1103/PhysRevLett.113.267602.
[22] S. Cheng, M. Li, Q. Meng, W. Duan, Y.G. Zhao, X.F. Sun, Y. Zhu, J. Zhu, Electronic and crystal structure changes induced by in-plane oxygen vacancies in multiferroic $YMnO_3$, Phys. Rev. B 93 (2016) 054409, https://doi.org/10.1103/PhysRevB.93.054409.
[23] A.S. Gibbs, K.S. Knight, P. Lightfoot, High-temperature phase transitions of hexagonal YMnO 3, Phys. Rev. B 83 (2011) 094111, https://doi.org/10.1103/PhysRevB.83.094111.
[24] N. Jiang, X. Zhang, Atomistic simulation study of transverse domain wall in hexagonal $YMnO_3$, J. Phys. D. Appl. Phys. 48 (2015) 435503, https://doi.org/10.1088/0022-3727/48/43/435503.
[25] B.B. Van Aken, T.T.M. Palstra, A. Filippetti, N.A. Spaldin, The origin of ferroelectricity in magnetoelectric $YMnO_3$, Nat. Mater. 3 (2004) 164–170, https://doi.org/10.1038/nmat1080.
[26] Y. Kumagai, A.A. Belik, M. Lilienblum, N. Leo, M. Fiebig, N.A. Spaldin, Observation of persistent centrosymmetricity in the hexagonal manganite family, Phys. Rev. B 85 (2012) 174422, , https://doi.org/10.1103/PhysRevB.85.174422.
[27] Z. Chen, X. Wang, S.P. Ringer, X. Liao, Manipulation of nanoscale domain switching using an electron beam with omnidirectional electric field distribution, Phys. Rev. Lett. 117 (2016) 027601, , https://doi.org/10.1103/PhysRevLett.117.027601.
[28] I.E. Graboy, A.A. Bosak, O.Y. Gorbenko, A.R. Kaul, C. Dubourdieu, J. Se, HREM study of epitaxially stabilized hexagonal rare earth manganites, Chem. Mater. 2 (2003) 2632–2637, https://doi.org/10.1021/cm021315b.
[29] A. Baghizadeh, J.M. Vieira, P. Mirzadeh Vaghefi, M.-G. Willinger, V.S. Amaral, Development of ferroelectric domains and topological defects in vacancy doped ceramics of h-$LuMnO_3$, J. Appl. Phys. 122 (2017) 044102, , https://doi.org/10.1063/1.4996349.
[30] S.-Z. Lin, X. Wang, Y. Kamiya, G.-W. Chern, F. Fan, D. Fan, B. Casas, Y. Liu, V. Kiryukhin, W.H. Zurek, C.D. Batista, S.-W. Cheong, Topological defects as relics of emergent continuous symmetry and Higgs condensation of disorder in ferroelectrics, Nat. Phys. 10 (2014) 970–977, https://doi.org/10.1038/nphys3142.